Int. J. Electrochem. Sci., 9 **(2014)** 3068 - 3077

International Journal of
ELECTROCHEMICAL
SCIENCE
www.electrochemsci.org

Precursor and Reaction Time Effects in Evaluation of Photocatalytic Properties of TiO_2 Nanoparticles Synthesized via Low Temperature

Ommeaymen Sheikhnejad-Bishe[1], *Feng Zhao*[1], *Ali Rajabtabar-Darvishi*[1], *Erfan Khodadad*[2] *and Yudong Huang*[1,*]

[1]Department of Polymer Science and Engineering, School of Chemical Engineering and Technology, Harbin Institute of Technology, Harbin 150001, People's Republic of China
[2] Surface Engineering Laboratory, School of Materials Science and Engineering, Dalian University of Technology, Dalian 116024, People's Republic of China
[*]E-mail: ydhuang.hit1@aliyun.com

Received: 30 January 2014 / *Accepted:* 26 February 2014 / *Published:* 23 March 2014

TiO_2 nanoparticles were synthesized by sol-gel method under low temperature via short crystallization time. The samples morphology, crystal size, specific surface area, pore size and particle size were significantly changed by varying the precursor concentration and the reaction time. The photocatalytic activities of the samples were evaluated by measuring the degradation of methyl orange under a 150W xenon lamp and compared to the photocatalytic activity of Degussa P25. Scanning Electron Microscopy and X-ray diffraction results show samples had uniform morphology, well crystalline structure and having the anatase phase. The maximum photocatalytic activity was achieved for the samples with the higher concentration of precursor (S2). The higher surface area and smaller crystal size played important roles in the degradation of the organic pollutants.

Keywords: Anatase TiO_2; Photocatalytic Activity; Sol-gel Preparation; Low temperature

1. INTRODUCTION

Titanium dioxide (TiO_2) is an environmentally benign material with unique optical and electrical properties, good chemical stability, high photoactivity [1, 2] and a large band gap [3, 4]. It has been applied as chemical sensing, energy conversion and degradation of pollutants in aqueous solutions by using UV light irradiation [5, 6]. TiO_2 was known to be a good photocatalyst due to its high photosensitivity, nontoxicity, easy availability, strong oxidizing power, and long-term stability [7]. Its photocatalytic properties strongly depend on surface area, phase composition and crystallinity.

These characteristics motivated many researchers to synthesize its nanostructures by various techniques such as hydrothermal, solvothermal, sol-gel process and electro-deposition [8, 9].

During the last three decades the sol-gel method is largely used for preparation of TiO_2 nanocrystals. Sol-gel is a solution-based technique, where material structure is created through chemical reactions in liquid state [10] and allows the formation of nanostructure materials with controlled shape in the form of powder or films [11]. It provides a simple and inexpensive way to prepare high active anatase photocatalyst.

In this research, we report the synthesis of anatase TiO_2 nanoparticles via sol-gel technique using the low temperature and reaction time. The influence of the experimental parameters such as reaction time and precursor ratio on the morphology and surface area of the samples were studied with a new approach and precision. The photocatalytic activity of the samples was analyzed through degradation of methyl orange (MO) and compared with the photocatalytic activity of P25.

2. EXPERIMENTAL SECTION

2.1. Sample Preparation

Tetrabutyl titanate (Ti $(OC_4H_9)_4$) was utilized as precursor, ethanol as the solvent, nitric acid as the catalyst and water for hydrolysis were provided by Sinopham Chemical Reagent Co. Ltd. and used as received without further purification. The typical procedures were described as follow:

Different amounts of nitric acid were added drop by drop into 34 ml ethanol under vigorous stirring. Then different concentrations of tetrabutyl titanate were slowly added to the solution and followed by stirring for 10 minutes. The obtained mixture was pale yellow in color. Then it was added to 150 ml distilled water drop wise under magnetic stirring at room temperature, and kept under vigorous stirring for 30 minutes. The obtained solution was treated at 50℃ in the oven for different time to complete crystallization. After the gelation, the wet gels were washed with distilled water and dried at 80℃. Finally, the powder was grinding to obtain fine powder for further study.

2.2. Characterization

Structural characterization of the materials were determined by X-ray diffraction (XRD), performed on RIGAK D/MAX-r-B. The average crystal size was determined by XRD peak broadening using the Scherrer equation:

$$t = \frac{K\lambda}{(\beta.\cos\theta)} \quad (1)$$

Where t is the average crystal size, $K(= 0.89)$ is the Scherrer constant, λ (=0.154118 nm) is the X-ray wave length, β is the peak width of half maximum, and θ is the Braggs diffraction angle. Microstructure and the morphology of the samples were analyzed using scanning electron microscopy (SEM, Hitachi S-3700). The adsorption-desorption Brunauer-Emmett-Teller (BET) surface areas were evaluated by nitrogen adsorption method (ASAP2020, Micrometrics). The average particle size was

measured by the following equation Eq. (2). In this equation (D) is the average particle size, $\rho\ (= 4.2\ g/cm^3)$ is the density of TiO_2 and S_{BET} was the specific surface area. The average particle size is estimated by assuming that the particles are spherical and they have a similar density.

$$D = \frac{6000}{(\rho S_{BET})} \quad (2)$$

2.3. Photocatalytic Activity Tests

Methyl orange was chosen to test the photocatalytic activities of the as-prepared catalysts. 0.04 g of the sample was dispersed into 40 ml MO (3×10^{-5} M) aqueous solution. The solution was magnetically stirred in the dark for 30 min to ensure the adsorption/desorption equilibrium. After illumination with a 150W xenon lamp, 6 ml of the solution were withdrawn at regular time and centrifuged at 11000 rpm for 9 min. As a comparison, the photocatalytic activity of P25 was also tested at the same condition. The degradation of MO was measured with a UV-752N PC spectrometer at a wavelength of 465 nm.

3. RESULTS AND DISCUSSION

3.1. Phase Construction, Morphology and Structures

Fig. 1 shows the XRD patterns of the synthesized samples and Table 1 shows the identification of the prepared samples. The presence of anatase and brookite in XRD patterns are identified according to the JCPDS files of #21-1272 and #29-1360, respectively. These results show that all the samples display the characteristic peaks of anatase and brookite, but most of the peaks belong to anatase and just the slight peak at 30.8° corresponds to brookite phase.

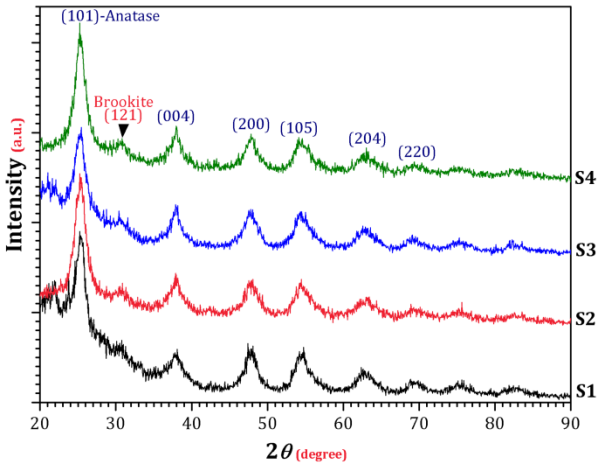

Figure 1. XRD patterns of different TiO_2 samples (S1-S4), results displayed the characteristic peaks of anatase and the phase at 30.8º corresponds to brookite phase. The phase at 53.9º corresponds to triangular crystalline lattice (105).

Table 1. Preparation materials, methods and crystal structures of TiO_2 samples.

Sample number	Content		Reaction time (h)	$\frac{I_{Brookite}}{I_{Anatase}}$ (%)
	Acid (ml)	Titanate (ml)		
S1	0.1	9.75	12	24
S2	0.1	19.5	12	12.5
S3	0.05	9.75	6	26
S4	0.05	9.75	12	13.4

As can be seen in Fig. 1, there is a triangular crystal lattice at 53.9º (105) for all the samples. The relative intensity of brookite pahse to anatase one were calculated using MDI Jade (version 6) software (Table 1), which indicates the lowest relative intensity for S2 and the highest one for S3. We were also calculated the relative intensity of triangular phase presence in XRD patterns that were 32.2, 27.6, 34.7 and 19.7% for S1-S4, respectively.

The SEM images show that the samples consist of uniform spherical particles with different sizes. Sample S1 has a great deal of spheres with different sizes which are assembled by small particles. The image depicts uniform distribution of the particles with high agglomeration (Fig. 2a). Most of the particles in S2 have homogeneous spheres with slight agglomeration (Fig. 2b). SEM images of S3 and S4 are shown in Fig. 2c and d, which are different in reaction time.

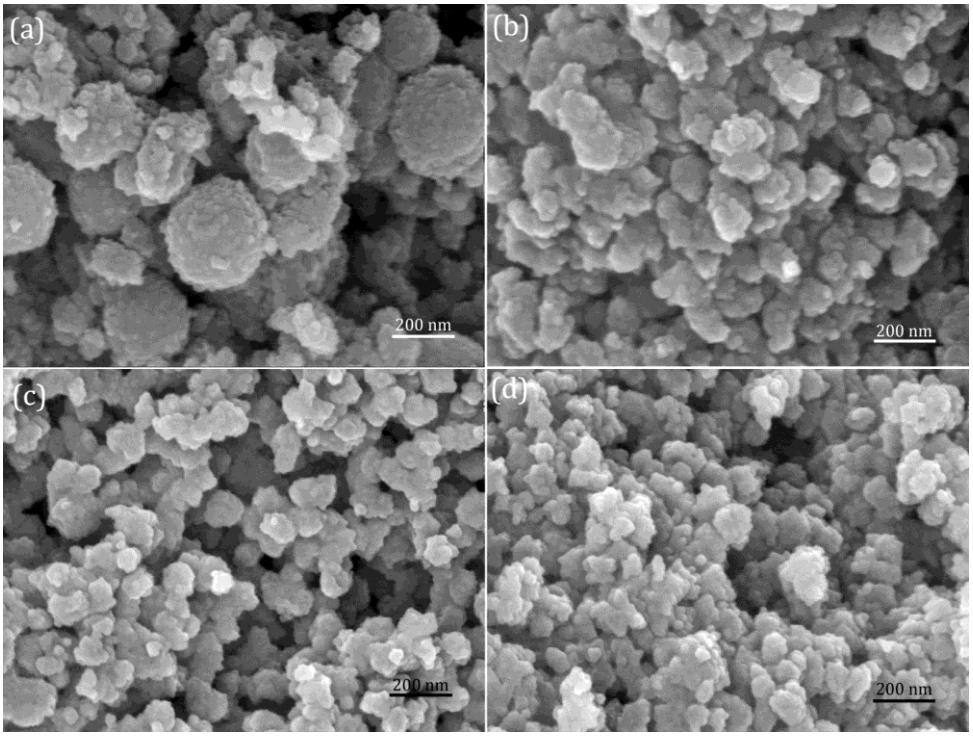

Figure 2. SEM images of different samples with preparation condition of (Acid ^{ml}, Titanat ^{ml}, Reaction time ^{h}): (a) S1-(0.1, 9.75, 12), (b) S2-(0.1, 19.5, 12), (c) S3-(0.05, 9.75, 6), and (d) S4-(0.05, 9.75, 12).

S3 possesses small particles with rough surfaces which are uniformly distributed throughout the samples. According to Fig. 2d, by prolonging reaction time in S4, the size of the spheres increased slightly due to the higher rang of agglomeration in the particles.

The variation of the crystal size and the particle size of the samples are given in Table 2, which were calculated using Eq. (1) and (2), respectively [12, 13]. The particle size obtained by BET method shows a similar trend as the crystal size calculated from Scherrer's equation. The average particle size of S1 was slightly more than its crystal size but for other samples these values are very close to each other. This is essentially attributed to the slight aggregation of the particles in this sample.

According to the results, S2 possesses the smallest size of both crystal size and particle size. At the reaction temperature of 50°C, the crystal size gradually grew when the reaction time increased from 6 to 12 h due to the further crystal growth [14]. It can be concluded that an increase in the particle size of TiO_2 is associated with the increase in the reaction time.

Table 2. Crystal size and particle size of the samples.

Sample	2θ (º)	FWHM (º)	Average crystal size (nm)	Average particle size (nm)
S1	25.28	1.30	6.22	6.76
S2	25.30	1.35	5.97	6.13
S3	25.23	1.24	6.48	6.58
S4	25.29	2.34	6.53	6.64

3.2. N2 adsorption-desorption analysis

Fig. 3 illustrates the nitrogen adsorption-desorption isotherms of the samples:

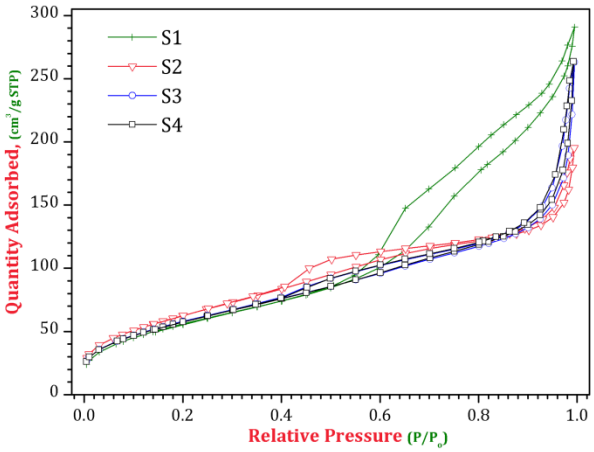

Figure 3. N_2 adsorption-desorption isotherm of as-prepared samples with preparation condition of (Acid [ml], Titanat [ml], Reaction time [h]): (a) S1-(0.1, 9.75, 12), (b) S2-(0.1, 19.5, 12), (c) S3-(0.05, 9.75, 6), and (d) S4-(0.05, 9.75, 12).

The specific surface area, pore size and pore volume calculated by BET and Barret-Joyner-Halenda methods that are listed in Table 3. According to the IUPAC classification the isotherms are identified as type IV with H3-type hysteresis loop [15], which are typically characteristic of porous materials [16, 17] consisting agglomerates or compacts of spherical particles [18]. According to Table 3, the specific surface area of all the samples is higher than P25. This might be due to the small growth of the particles during the sol-gel method at the low temperature which produces the particles with smaller pore diameter than P25.

Table 3. Textural properties of different TiO_2.

Sample	BET surface area ($m^2.g^{-1}$)	Average pore diameter (Å)	Total pore volume ($cm^3.g^{-1}$)
P25	51.37	86.27	0.110
S1	211.138	73.87	0.389
S2	232.911	40.33	0.234
S3	216.796	48.92	0.265
S4	215.012	51.11	0.274

Comparing S1 and S2 specimens indicates that the particles coagulate together with an increase in the precursor concentration and the size of the particles slightly decreases which leads to an increase in the specific surface area. With prolonging the reaction time (comparing S3 and S4), the specific surface area is slightly decreased. This fact evidences that increasing the crystallization of the particles leads to the further growth of them and decreases the specific surface area [19].

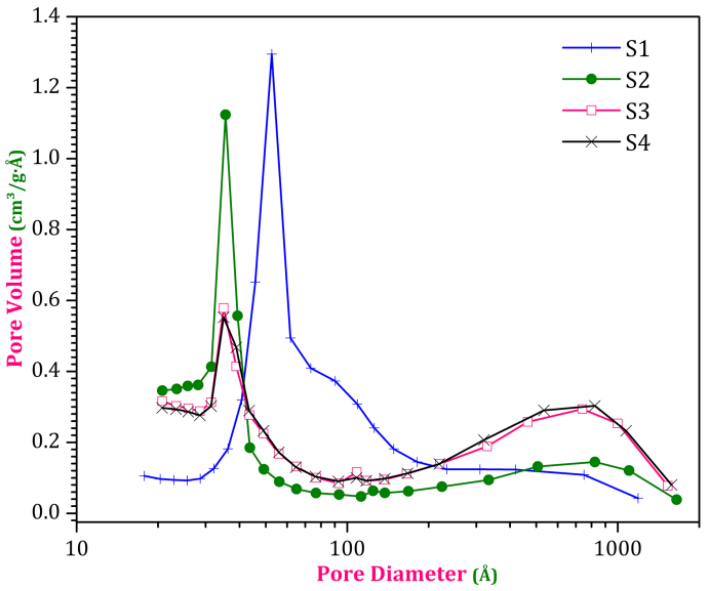

Figure 4. Pore size distribution of different as-prepared samples.

Fig. 4 shows the pore size distribution of the samples. All of the samples possess narrow distribution which indicates the mesoporous structure [20]. According to the results, S1 possesses the greatest number of pores and S2 contains the smallest pores. As the result showed, S2 possessed the highest specific surface area and it is expected to have a wider application in photocatalysis. BET analysis revealed that the specific surface area of the powders decreased with an increase of the pore size of the samples.

3.3. Photocatalytic activity

The results of the photocatalytic activity of as-prepared samples are presented in Fig. 5. The photocatalytic property of P25 was measured as a reference. The degradation of MO is monitored by examining the variations in UV-visible spectra at 465 nm.

Photocatalysis is a phenomenon which occurs on the surface and it contains the absorption of the organic compounds on the surface of the photocatalyst [21]. It has been reported that photocatalytic activity of TiO_2 depends on surface area, crystal size, crystal structure, and temperature [9]. Elimination of MO can be affected by the absorption of the dye on the active sites of the surface.

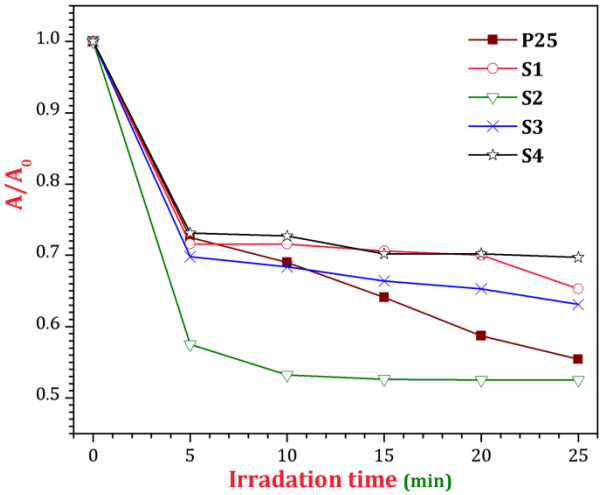

Figure 5. Absorption of methyl orange for different as-prepared samples and P25 during the irradiation time.

In the photodegradation process, the electrons are excited from the valence band (VB) to the conduction band (CB) with the absorption of photons and creating holes (h^+) at the VB band. In the CB, the excited electrons transfer to the adsorbed O_2 on the surface of TiO_2 to form the superoxide radical onions $(\dot{O}_2^-)$ and the holes in the VB can form hydroxyl radical $(\dot{O}H)$ by the interaction with water molecules [22]. The protonation of the $(\dot{O}_2^-)$ creates $\dot{O}OH$ which leads to the formation of H_2O_2 and finally $\dot{O}H$ radical. The hydroxyl radicals react with MO and oxidize them into non-pollution products. The mechanism of the degradation can be expressed as following Eq. 3-7:

$$TiO_2 + h\nu \rightarrow e^- + h^+ \quad (3)$$

$$h^+ + H_2O \rightarrow \dot{O}H + H^+ \quad (4)$$

$$O_2 + 2e^- + 2H^+ \rightarrow H_2O_2 \quad (5)$$

$$H_2O_2 \rightarrow 2\dot{O}H \quad (6)$$

$$MO\ Dye + \dot{O}H \rightarrow Degradation\ Products \quad (7)$$

According to the results, the absorption ability of the samples for MO decreased with prolonging irradiation time, indicating that all the samples indeed possess photocatalytic function. The MO decoloration was caused by degradation of the conjugative system consists of azo group and aryl ring [19].

The excellent adsorption ability facilitates the diffusion of MO molecule from solution to the surface of the catalysts and improves the photocatalytic property. As it shown in Fig. 5, the best absorption ability of MO is found at S2 and the worst absorption appeared at S4. Comparing with P25, the results of S2 have better MO elimination than P25. It means that the absorption of the organic molecules on the surface of S2 is favorable and facilitates the enhancement of dye degradation. As a result, it possessed an excellent photocatalytic activity. It is suggested that the particles coagulate together with increasing of precursor concentration, so the size of the particles decreased which may lead to increasing the specific surface area and provide more active sites to promote the adsorption capacity. Moreover, S2 has larger pore volume than P25 which acts as the catalytic site for degradation of the organic pollutant. As observed in XRD result, S2 possessed low relative intensity of brookite phase and triangular crystal lattice, which may lead to prominent increase in the photocatalytic property.

Comparison between S3 and S4 indicates that prolonging the reaction time leads to more agglomeration of the particles and results in the reduction of the availability of active sites. Hence, the active sites of the catalyst surface become unavailable for dye adsorption, so the photodegradation of the organic pollution decreases. Although the specific surface area of S1, S3 and S4 was more than P25 but the photodegradation efficiency of P25 was more than them. It is known that P25 has a small surface area with the small particles and high crystallization rate, so these properties are beneficial for adsorption of MO [23]. Finally, it should be pointed out that the photodegradation of S2 is better than P25, which attributed to higher specific surface area and smaller particle size. In addition, the factors that may contribute towards higher activity for the samples are: (1) high surface area, which could provide more active sites for dye adsorption, and (2) small crystal size, which leads to the fast charge migration from balk to the surface of the catalyst.

4. CONCLUSIONS

We have demonstrated that anatase TiO_2 samples with high photocatalytic activity can be produced by a short crystallization time and low temperature (50°C) via the simple and inexpensive sol-gel method. The synthesis doesn't need any structure-directing or surfactant and it can be accelerated by applying oven. At very low temperature, the nanocrystals formation were strongly

showed that all the samples consist of agglomerated particles. In this work, reaction time and the concentration of the precursor play the chief roles in the structure and the morphology of the particles. Due to the relatively large surface area and small particle size, the best photodegradation of MO was obtained by using the sample which prepared at higher precursor concentration. Particle size plays a vital role in photocatalytic activity since smaller crystals offered greater surface area to volume ratios, induced better surface absorbability of hydroxyl and lowered the electron hole recombination.

Based on this study, we inferred that the specific surface area, crystal size, crystallinity, particle size, absorption of dye on the surface and the electron hole recombination rate play very important roles to improve the photocatalytic activity of synthesized TiO_2 nanoparticles. Crystallization with the lowest temperature, short reaction time and utilizing different precursor concentration are the most important technical advantages of current work. The synthesized TiO_2 structure is suitable to apply in surface reaction devices such as solar cell and photochromic devices.

ACKNOWLEDGMENT
The authors gratefully acknowledge the supports from the Changjiang scholars program and the national Nature Science Foundation of China (No. 51073047 and No. 91076015).

References

1. Y. Zhang, Z. R. Tang, X. Fu, and Y. J. Xu, *Acs Nano*, 4 (2010) 7303.
2. F. Fang, L. Chen, Y. B. Chen, and L. M. Wu, *J. Phys. Chem. C*, 114 (2010) 2393.
3. T. K. Kim, E. D. Jeong, M. S. Lee, J. P. Kim, M. H. Hyun, O. S. Jung, H. Suh, F. N. Khan, and J. S. Jin, *Res. Chem. Intermed.*, 38 (2012) 685.
4. R. Thapa, S. Maiti, T. H. Rana, U. N. Maiti, and K. K. Chattopadhyay, *J. Mol. Catal. A: Chem.*, 363–364 (2012) 223.
5. B. Mazinani, A. Beitollahi, A. K. Masrom, N. Yahya, T. S. Choong, S. M. Ibrahim, and J. Javadpour, *Res. Chem. Intermed.*, 38 (2012) 1733.
6. N. Zhang, Y. Zhang, and Y. J. Xu, *Nanoscale*, 4 (2012) 5792.
7. M. Saif, S. Aboul-Fotouh, S. El-Molla, M. Ibrahim, and L. Ismail, *J. Nanopart. Res.*, 14 (2012) 1.
8. Y. C. Hsu, H. C. Lin, C. H. Chen, Y. T. Liao, and C. M. Yang, *J. Solid State Chem.*, 183 (2010) 1917.
9. X. H. Xia, Y. Liang, Z. Wang, J. Fan, Y. S. Luo, and Z. J. Jia, *Mater. Res. Bull.*, 43 (2008) 2187.
10. M. Šćepanović, B. Abramović, A. Golubović, S. Kler, M. Grujić-Brojčin, Z. Dohčević-Mitrović, B. Babić, B. Matović, and Z. V. Popović, *J. Sol-Gel Sci. Technol.*, 61 (2012) 390.
11. S. Valencia, X. Vargas, L. Rios, G. Restrepo, and J. M. Marín, *J. Photochem. Photobiol., A-Chem*, 251 (2013) 175.
12. M. A. Behnajady, N. Modirshahla, M. Shokri, H. Elham, and A. Zeininezhad, *J. Environ. Sci. Health., Part A*, 43 (2008) 460.
13. S. Agarwala, M. Kevin, A. Wong, C. Peh, V. Thavasi, and G. Ho, *ACS Appl. Mater. Interfaces*, 2 (2010) 1844.
14. X. Wang, L. Cao, D. Chen, and R. A. Caruso, *ACS Appl. Mater. Interfaces*, 5 (2013) 9421.
15. S. Naumov, "Hysteresis Phenomena in Mesoporous Materials," PhD thesis, Universitat Leipzig, Germany, 2009.
16. Y. g. Tao, Y. q. Xu, J. Pan, H. Gu, C. Y. Qin, and P. Zhou, *Mater. Sci. Eng., B*, 177 (2012) 1664.
17. D. A. Kumar, J. A. Xavier, J. M. Shyla, and F. P. Xavier, *Mater. Sci.*, 48 (2013) 3700.
18. N. I. Ermokhina, V. A. Nevinskiy, P. A. Manorik, V. G. Ilyin, N. N. Shcherbatyuk, D. O. Klymchyuk, and A. M. Puziy, *Mater. Lett.*, 75 (2012) 68.

19. Z. Wang, C. Chen, F. Wu, B. Zou, M. Zhao, J. Wang, and C. Feng, *J. Hazard. Mater.*, 164 (2009) 615.
20. S. Chu, L. Luo, J. Yang, F. Kong, S. Luo, Y. Wang, and Z. Zou, *Appl. Surf. Sci.*, 258 (2012) 9664.
21. N. Riaz, F. K. Chong, B. K. Dutta, Z. B. Man, M. S. Khan, and E. Nurlaela, *Chem. Eng. J.*, 185 (2012) 108.
22. S. Padikkaparambil, B. Narayanan, Z. Yaakob, S. Viswanathan, and S. M. Tasirin, *Int. J. Photoenergy*, 2013 (2013)
23. H. Feng, M. H. Zhang, and L. E. Yu, *Appl. Catal. A*, 413–414 (2012) 238.